

Dalton Transactions

Accepted Manuscript



This is an *Accepted Manuscript*, which has been through the Royal Society of Chemistry peer review process and has been accepted for publication.

Accepted Manuscripts are published online shortly after acceptance, before technical editing, formatting and proof reading. Using this free service, authors can make their results available to the community, in citable form, before we publish the edited article. We will replace this *Accepted Manuscript* with the edited and formatted *Advance Article* as soon as it is available.

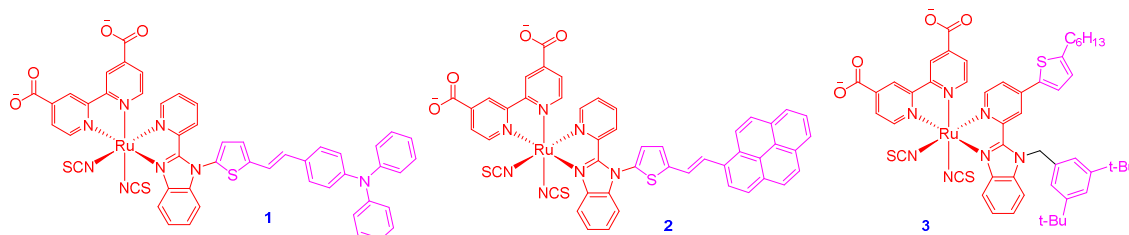
You can find more information about *Accepted Manuscripts* in the [Information for Authors](#).

Please note that technical editing may introduce minor changes to the text and/or graphics, which may alter content. The journal's standard [Terms & Conditions](#) and the [Ethical guidelines](#) still apply. In no event shall the Royal Society of Chemistry be held responsible for any errors or omissions in this *Accepted Manuscript* or any consequences arising from the use of any information it contains.

Graphical Abstract

Benzimidazole functionalized ancillary ligands for heteroleptic Ru(II) complexes: synthesis, characterization and dye-sensitized solar cell applications

Tejaswi Jella,^a Malladi Srikanth^b Rambabu Bolligarla^a Yarasi Soujanya,^b Surya Prakash Singh^a and Lingamallu Giribabu^{a*}



We have designed three new heteroleptic Ru(II) polypyridyl complexes having pyridine-benzimidazole (pyridine-BI) functionalized ligand for dye-sensitized solar cells. The complex having substituents both at position A and B of pyridine-BI ligand have shown an efficiency of 7.88% using I⁻/I₃⁻ redox couple. Under similar test cell conditions N719 shown an efficiency of 8.02%.



Journal Name

ARTICLE

Benzimidazole functionalized ancillary ligands for heteroleptic Ru(II) complexes: synthesis, characterization and dye-sensitized solar cell applications

Received 00th January 20xx,
Accepted 00th January 20xx

DOI: 10.1039/x0xx00000x

www.rsc.org/

Tejaswi Jella,^a Malladi Srikanth,^b Rambabu Bolligarla,^a Yarasi Soujanya,^b Surya Prakash Singh^a and Lingamallu Giribabu^{a*}

We have designed and synthesized heteroleptic Ru(II) complexes having pyridine-benzimidazole ligand (PYBI) for dye-sensitized solar cell (DSSC) applications. The PYBI ligands has major advantage by having flexibility to introduce proper substituents at readily available four positions through molecular engineering (chart 1) compared to other ancillary bipyridyl based ligands. We have substituted position A of PYBI ligand by either electron releasing triphenylamine (**1**) or pyrene (**2**). We have also introduced 2-hexylthiophene at position A and 3,5-di *tert*-butyl phenyl group at position B of PYBI (**3**) ligand. All three heteroleptic Ru(II) complexes have been characterized by Mass, ¹H NMR, absorption and emission spectroscopies as well as electrochemical methods. Absorption spectra of complex **3** is red-shifted and emission spectra is blue-shifted, when compared to standard **N719** sensitizer. Testing of these newly designed heteroleptic Ru(II) sensitizers has revealed that the complex **3** exhibit an efficiency of 7.88% using I⁻/I₃⁻ redox electrolyte. Experimental observations corroborated with computational calculations have elucidated the high efficiency of complex **3**, primarily due to substituents at position A are influential than at position of B of PYBI ligand.

Introduction

Dye Sensitized Solar Cells (DSSCs) are promising for the next generation photovoltaic devices over conventional silicon based solar cells largely due to their negligible sensitivity to impurities, easy to fabrication by techniques like screen printing, spraying and pressing, improved stability over a wide range of temperature, flexibility in choosing the substrates utilized which on the whole leads to low cost of production.¹⁻³ Furthermore, the leading advantages of DSSCs are works well at diffuse light conditions compared to the trademark solid state silicon photovoltaics.⁴ DSSC has reached certified efficiency of >11%. However, before commercialization of the technology almost all components of the device have to be improved. Among various components, the sensitizer is one of the vital component to improve the efficiency and durability of the device. During last two decades, various photosensitizers for DSSC such as ruthenium dyes,⁵⁻⁷ tetrapyrrolic sensitizers (zinc porphyrin and phthalocyanines),⁸⁻¹² and metal-free organic dyes¹³⁻¹⁵ have been developed to serve as efficient harvesters

of sun light. Very recently, a new concept has been developed on perovskite based DSSC that has shown an efficiency of up to 20.1%.¹⁶ However, the durability of the sensitizer for real outdoor long-term applications is still significant challenge.

Ruthenium complexes have been remaining particularly interested as photosensitizers in DSSC for the practical feasible applications due to their favourable photoelectrochemical properties and high stability in the oxidized state.¹⁷ DSSC devices has been constructed by using homoleptic ruthenium sensitizers (**N3**, **N719** and black dye) were achieved an efficiency of up to 11% under standard AM 1.5 illumination and stable operation for millions of turnovers.^{5-7,18} To enhance the durability of the device, ruthenium analogue, **Z907** has been developed. However, despite having greater durability compared to **N3** and **N719**, efficiency of **Z907** is found to be poor because of its low molar absorption.^{19,20} In this context, one of the ways to increase the PCE (η) and durability of the test cell device is through high molar extension coefficient, by introducing an extended π -conjugation structures of thiophene substituted at the bipyridine moiety in heteroleptic manner. Many of the thiophene based heteroleptic ruthenium dyes with significantly improved efficiencies and stability of the test cell devices were reported.²¹⁻²⁵ For example **C101** and **C102** sensitizers showed PCE(η) above 11.5 % with good molar extension coefficient values.²¹⁻²⁵ Recently Diao and co-workers reported by using the concept of

^a *Inorganic & Physical Chemistry Division, CSIR-Indian Institute of Chemical Technology, and CSIR-Network Institutes for Solar Energy (CSIR-NISE), Tarnaka, Hyderabad-500007, (Telangana), India .Email: giribabu@iict.res.in. Phone: +91-40-27191724, Fax: +91-40-27160921*

^b *Center for Molecular Modeling, CSIR-Indian Institute of Chemical Technology, Hyderabad 500007, India.*

^c * Footnotes relating to the title and/or authors should appear here.

Electronic Supplementary Information (ESI) available: [ESI-MS, ¹H NMR spectral data of all compounds and tables of molecular orbital composition and calculated absorption spectral wavelength data are available should be included here]. See DOI: 10.1039/x0xx00000x

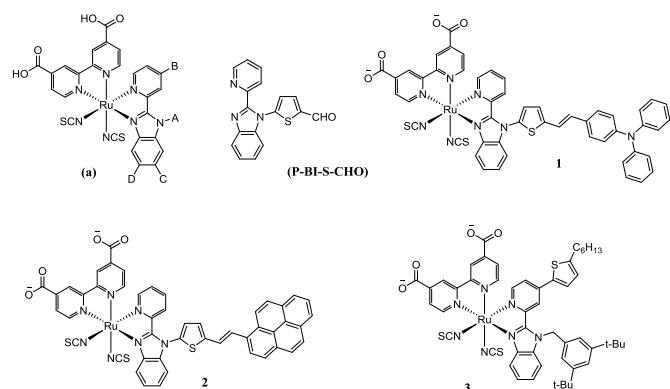
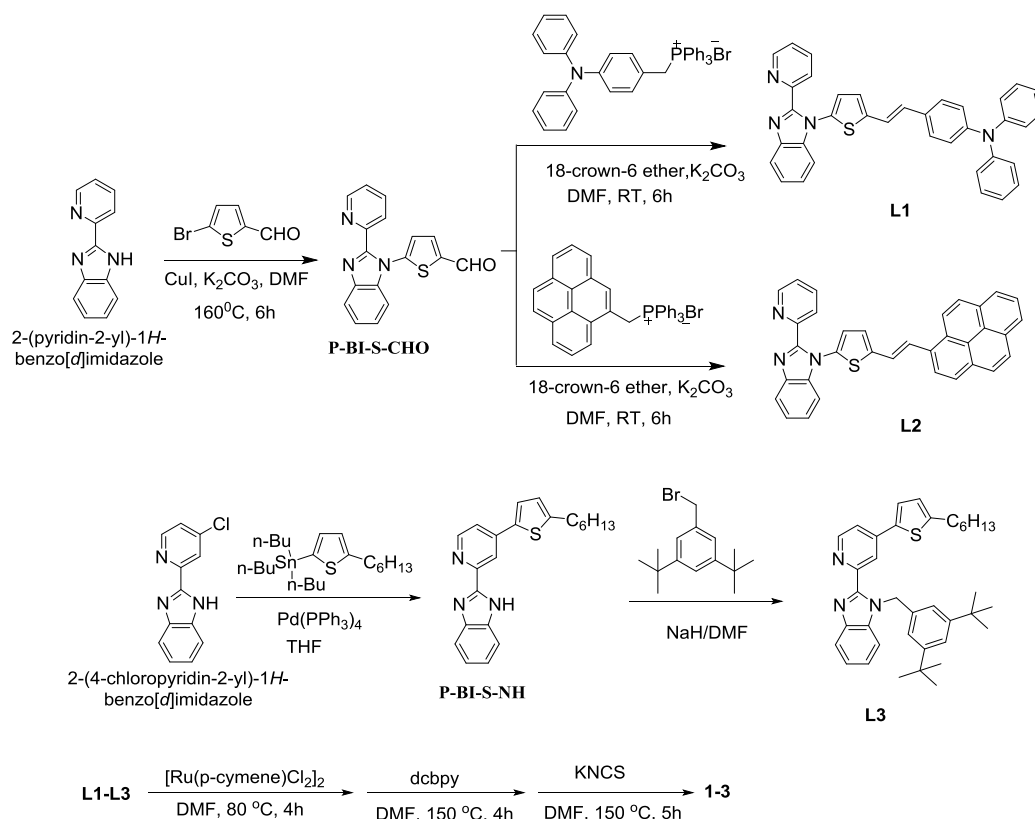


Chart 1. Possible positions for structural modification in heteroleptic Ru-complex containing the PYBI ligand; Newly synthesized BI-formylated thiophene precursor for various structural modification of pyridine-BI at α -position thiophene derivative and ruthenium complexes **1-3**.

thiophene groups introduced to the pyridine-benzimidazole ligands at B position as shown in Chart 1.²⁶ These thiophene based pyridine-benzimidazole ligands (PYBI) containing heteroleptic ruthenium sensitizers **RD16-RD18** have displayed enhanced PCE (η) and short circuit current density (J_{sc}) comparable to that of **N719** dye, which is attributed to the broad spectral features in the low energy region. Moreover, these PYBI ligands having greater advantageous of more flexibility for structural modification through proper molecular engineering to endorse further device performance at readily available four positions compared to other ancillary bipyridyl based ligands.

Additionally, PYBI derivatives have been developed as layer materials for electron transport and hole blocking in OLED devices because of their greater electron mobility, and also used as electrolyte additive in DSSC for enhancing the open-circuit voltage (V_{oc}).^{27,28}

In the continuation of our efforts towards the design of heteroleptic Ru-based sensitizers,²⁹⁻³¹ we have introduced formylated-thiophene derivative at position A (Chart 1) to the pyridine-benzimidazole ligand in a simple two step procedure. The present strategy of synthesis leads to various structural modification of PYBI at α -position of thiophene derivative to promote device performance further. In this regard, we have synthesized and characterized two new heteroleptic ruthenium(II) complexes containing highly electron donating TPA (triphenylamine) or pyrene connected through ethenyl spacer thiophene based PYBI ligand (Scheme 1). The electron releasing groups on extended π -conjugation of a PYBI ligand to increase the molar extinction coefficient, a bipyridine ligand with anchoring carboxyl groups to attach onto the TiO_2 surface and a thiocyanate ligand to tune the redox properties of the ruthenium centre. In addition to these, we have also synthesized a new thiophene substituted heteroleptic ruthenium(II) complex at position B (Chart 1). We report herein, the synthesis and spectroscopic, electrochemical, and photovoltaic properties of these three heteroleptic sensitizers using liquid iodide/triiodide based



Scheme 1. Synthetic route for the synthesis PYBI ligands (**L1-L3**) and Ru-BI complexes (**1-3**).

electrolyte. To gain insight into the electronic structure and properties of **1-3**, computational calculations using Density Functional Theory (DFT) have been carried out.

Results and Discussion

The important precursor compound **P-BI-S-CHO** was accomplished by nucleophilic substitution reaction of unsubstituted PYBI with 5-bromothiophene-2-carboxaldehyde in presence of base catalyst. This precursor **P-BI-S-CHO** could be used for the synthesis of ligands (**L1-L2**) by using Wittig reaction.³² The ligand **L3** was achieved by Stille coupling reaction of 2-(4-chloropyridin-2-yl)-1H-benzimidazole with tributyl(5-hexylthiophen-2-yl)stannane followed by nucleophilic substitution of 3,5-di-*t*-butylbenzyl bromide in presence of strong base.³³ All three ligands were characterized by ¹H NMR, Mass spectroscopy and CHN analysis (see *Experimental & Supporting information*). Finally ruthenium complexes **1-3** were synthesized by a typical one pot synthesis as shown in Scheme 1. All new heteroleptic ruthenium sensitizers were purified by sephadex (LH-20) column using chloroform and methanol mixture as eluent. Preliminary characterization of these complexes were carried out by elemental analyses and mass spectroscopy. The mass spectra of all three ruthenium complexes consists of a molecular ion peak that corresponds to proposed structure (see *Supporting information*). The proton NMR spectrum of the Ru-dyes **1-3** show little complex spectra for characterization because they contain two diastereomers (observed as equal intensity) that cannot be separated by using column chromatography.³⁴ Consequently, the average effect of the two inseparable diastereomers should be considered for the results discussed in the following. Yun Chi *et al.* have isolated of all three possible isomers of -NCS free ruthenium(II) polypyridyl complexes and they demonstrated that mixture of optical isomers does not much effect on the device efficiency.^{35,36}

The absorption and emission spectra complexes **1-3** are measured in acetonitrile solvent at room temperature along with standard **N719** sensitizer are shown in Figure 1. Also depicted in the same figure, the simulated absorption spectra of these systems obtained from TD-DFT calculations. The

corresponding photophysical characterization data is summarized in Table 1. Inspection of Figure 1 and data in Table 1 reveals that the absorption features of the complexes **1-2** are almost identical in the low energy region (¹MLCT bands) electron donating either TPA (triphenylamine) or pyrene moieties connected through ethenyl spacer thiophene. The increase in molar absorption coefficients for these dyes is mainly due to electronic features of highly conjugated and are comparable with **N719** sensitizer. However, absorption bands at 400 nm are observed with large molar extinction PYBI ligand. In contrast, the absorption spectra of complex **3** show MLCT bands are shifted towards longer wavelength region as similar to the previous reported compounds^{26,34} compared to **N719**. This clearly indicating that the thiophene derivatives substituted at position B to the PYBI ligand influencing the MLCT absorption spectral features extended to red region compared to thiophene derivatives substituted at position A to the PYBI ligand which does not influence MLCT absorption spectral feature. Figure 1 also illustrates the emission spectra of complexes **1-3** along with **N719** sensitizer. Excitation of lower energy MLCT transition of complex **1** showed an emission maxima 20 nm red-shift in comparison with emission maxima

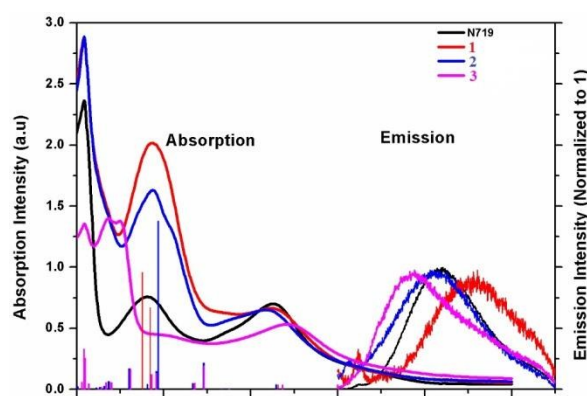


Figure 1. Absorption (left) and emission (right) spectra of ruthenium complexes **1** (2.6×10^{-5} M), **2** (2.64×10^{-5} M), **3** (2.6×10^{-5} M), and **N719** (3.78×10^{-5} M) in acetonitrile. Simulated absorption bands are shown as vertical bars.

Table 1. Absorption and electrochemical data.

Dye	$\epsilon_{\pi-\pi^*} (\lambda_{\max})$	$\epsilon_{\pi-\pi^*} (\lambda_{\max})$	$\epsilon_{\text{MLCT}} (\lambda_{\max})$	$\lambda_{\text{em}}, \text{nm}$	E_{0-0}^b / eV	$E_{\text{HOMO}}^a / \text{V}$	$E_{\text{LUMO}}^c / \text{V}$
1	57600 (308)	40360 (387)	13280 (524)	755	1.79	0.97	-0.82
2	57780 (308)	32620 (388)	13020 (517)	708	1.81	0.96	-0.85
3	33875 (309)	34950 (337) 34475 (349)	13325 (542)	680 722	1.84	0.77	-1.07 -0.88
N719	47300 (308)	15160 (381)	14020 (526)		1.85	0.97	-0.88

^aOxidation potential E_{HOM} (V vs. SCE) were measured for dyes in dry DMF in the presence of 0.1 M (n-C₄H₉)₄NPF₆. ^b E_{0-0} was determined from the intersection of absorption and emission spectra as shown in figure. ^c E_{LUMO} was determined as $E_{\text{ox}} - E_{0-0}$.

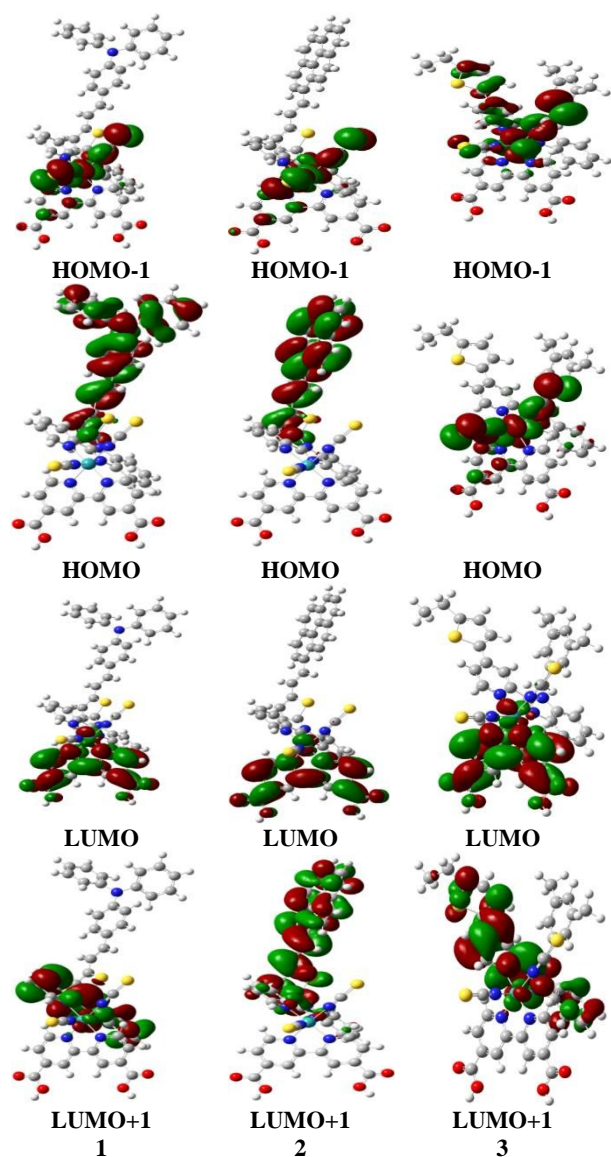


Figure 2. Molecular orbitals of HOMO, HOMO-1, LUMO, LUMO+1 for **1-3** calculated at CAM-B3LYP/6-311+G(d,p):LanL2DZ level of theory in acetonitrile.

of **N719** sensitizer. Whereas complex **3** exhibit blue shift in emission maxima. Based on the optical properties, $E_{0,0}$ energy of complexes **1-3** are found to be 1.79, 1.81 and 1.84 eV, respectively.

To gain insight into the structural, electronic and optical properties of the considered Ru(II) heteroleptic compounds, we carried out DFT and TD-DFT calculations. As shown in Figure 2, from the optimized geometries of **1-3**, the thienyl group is orthogonal when substituted at A site of BI unit, due to the greater steric interference exerted by BI unit. In contrast, the thienyl group on pyridine of complex **3** seems to be planar and participate in the extended π -conjugation as a result red-shift of the absorption maxima. The electron density distributions of the

frontier molecular energy levels HOMO, HOMO-1, LUMO and LUMO+1 for complexes **1-3** are depicted in Figure 2. In order to create an efficient charge separated state, HOMOs must be localized on the donor unit, and LUMOs must be on the acceptor and anchoring groups. As seen from the Figure 2 and Table S1, the electron densities of the highest occupied molecular orbitals, HOMO and HOMO-1 for **3** are mainly located at the ruthenium metal with contribution of 50 and 52% respectively, and the NCS ligands character is about 35%. For compounds **1** and **2** HOMO entirely localized on triphenylamine and pyrene and HOMO-1 has ruthenium metal with contribution of about 50%, and the NCS ligands character is about 35%. The lowest unoccupied molecular orbital (LUMO) of **1-3** have amplitude mostly on the anchoring bipyridyl ligand.

The calculated vertical excitation energies for singlet and triplet excited states, together with the calculated oscillator strengths are reported in Table S2. It is well known that among heteroleptic Ru-based sensitizers, the electron injection take place from $^1\text{MLCT}$ and $^3\text{MLCT}$ (S-T).^{6,37} Spin-forbidden $^3\text{MLCT}$ transition will depend on the energy gap between two excited states and will also depend on the spin-orbit coupling matrix element connecting the triplet and singlet states.³⁸ The calculated S-T gap is found to be much lower in **3** than for **1** &

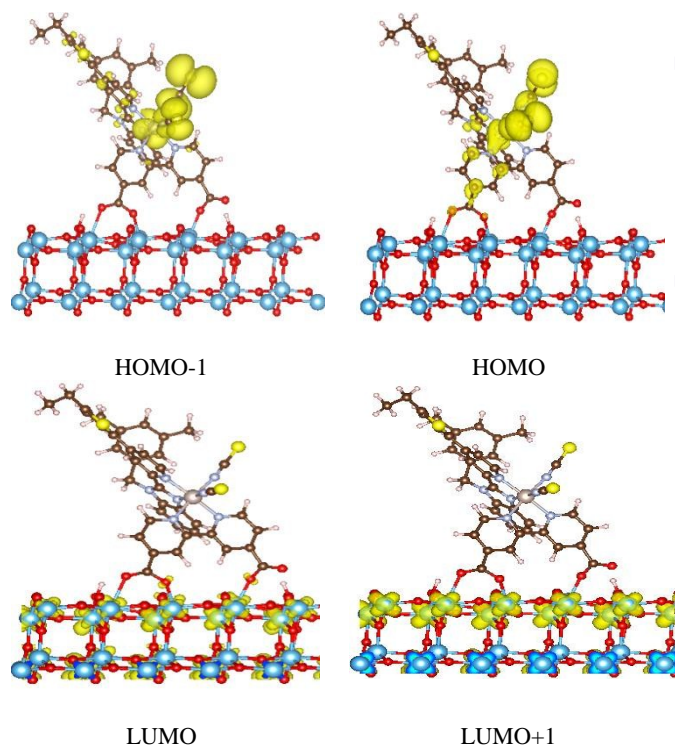


Figure 3. Partial charge densities of **3** anchored to anatase (101) for the eigen states of the two highest occupied and two lowest unoccupied crystalline orbitals for the Gamma point, gold colour indicates localization of electron density. These figures were plotted using VESTA.⁴¹

2. The MO contributions to major transitions as given in Table S2 also substantiate that the HOMO-LUMO transition which is from MLCT state involves the triplet state for **3**. From the TDDFT electronic transition analysis, (Table S2) ³IL (intra ligand) and ¹IL excited states are dominant for the Ru complexes appended with triphenyl amine (**1**) and pyrene (**2**) ligands. Another interesting observation from the Figure 2 is that in spite of well separated charge species in the complexes of **1** and **2**, the corresponding low V_{oc} values points to poor regeneration of dye. This is in agreement with similar observations made for ruthenium bipyridyl dyes, wherein the long-lived charge-separated state lead to extremely low DSSC efficiencies.^{39,40} All these observations explain the high efficiency of sensitizer **3** as due to efficient charge separation, improved charge injection and reduced charge recombination. This is in similar lines with the work of Daiu *et al* on the involvement of a benzimidazole ligand in heteroleptic ruthenium(II) polypyridyl dyes.³⁷

To investigate the binding orientation of most promising dye, **3** on TiO₂ surface, we have employed generalized gradient approximation (GGA) with the PBE functional and details of dye-TiO₂ adsorption calculations are given in following section. As clear from Figure 3, the dye is bound in two-arm mode to the TiO₂ surface with one of the carboxylic group binds through a monodentate mode and other anchoring group in bidentate binding with proton transfer to a nearby surface oxygen. Also it is clear that the HOMOs are delocalized over the dye, while the LUMOs are distributed at the TiO₂-dye interface, indicating the strong coupling between the injecting state of dyes and the CB of TiO₂.

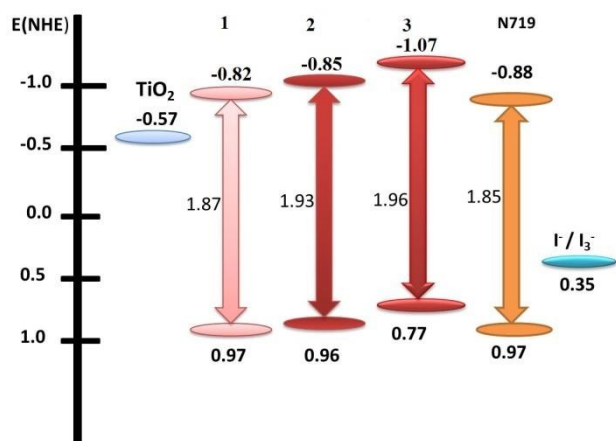


Figure 4. HOMO and LUMO levels obtained from electrochemical measurements.

The electrochemical properties of these Ru dyes were investigated by using differential pulse voltammetric (DPV) method with an internal reference of Fc/Fc⁺ couple. The redox potential data of complexes **1-3** along with standard **N719** sensitizers are presented in Table 1 and the corresponding DPV in supporting information.

For each sensitizer, the potential level of HOMO with respect to a normal hydrogen electrode (NHE) was determined $E_{\text{HOMO}} = E_{\text{OX}} - E_{\text{Fc/Fc}^+} + 0.64$, and the potential level of LUMO was determined from $E_{\text{LUMO}} = E_{\text{HOMO}} - E_{0-0}$;³⁴ the values of HOMO and LUMO are given in Table 1. Figure 4 shows an energy-level diagram of new heteroleptic Ru(II) sensitizers along with **N719** sensitizer for comparison of HOMO-LUMO levels of each sensitizer with respect to TiO₂ conduction band and the redox potential of I⁻/I₃⁻ redox couple. The energy-level diagram shows that the LUMO levels of these sensitizers become increasingly stabilized having substituents on both A and B positions in comparison substituents at position A of PYBI ligand, owing to the electron releasing nature of the substituents. All these heteroleptic Ru(II) sensitizers designed here, both electron injection and electron regeneration are feasible when they serve as sensitizers for DSSC.

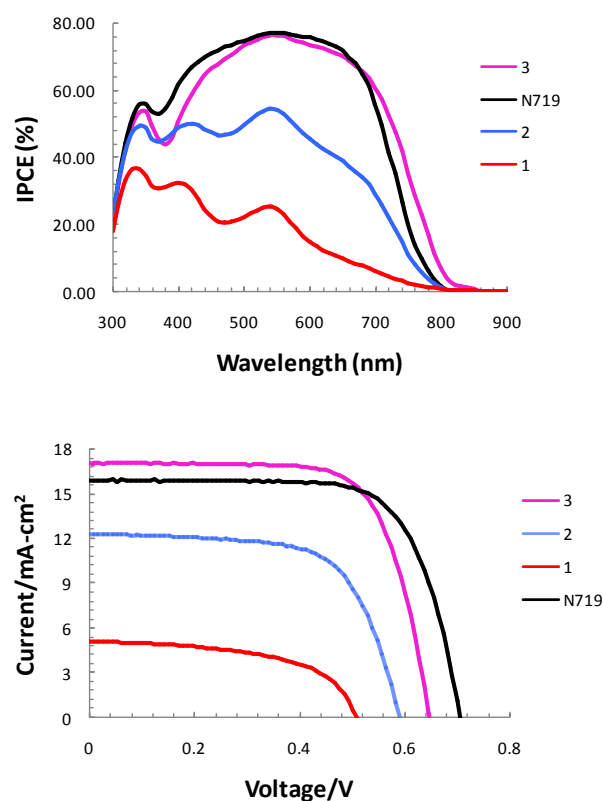


Figure 5(a) Photocurrent action spectra and **(b)** Current-voltage characteristics of complexes **1-3** and **N719**.

The newly designed heteroleptic Ru(II) sensitizers anchored onto a double layer nanocrystalline TiO₂ film and measure its photovoltaic properties using liquid redox electrolyte (I⁻/I₃⁻). Table 2 illustrates photovoltaic performance characteristics of complexes **1-3** along with standard **N719** sensitizer. Figure 5a shows the IPCE spectra of all three sensitizer and **N719** dye. We have observed maximum IPCE value of 78, 55 and 25% of complexes **3**, **1** and **2**, respectively at around 540 nm, indicating high dye loading for **3** more than **1** and **2**. Under similar test cell conditions, we have observed an IPCE of 78% for standard **N719** sensitizer. The photocurrent action spectrum resembles the absorption spectra except for a slight red shift by ca. 15 nm. The photoresponse of thin

films displays a broad spectral response covering the entire visible spectrum up to 800 nm. From the overlap integral of this curve one measures a short-circuit photocurrent density of 17.09, 12.35 and 5.14 ± 0.20 mA/cm² using complexes **3**, **1** and **2**, respectively. Figure 5b shows current-voltage characteristics of the devices using new heteroleptic Ru(II) sensitizers along with the **N719** sensitizer. Under standard global Air Mass (AM) 1.5 solar condition, complex **3** sensitizer based cell gave a short-circuit photocurrent density (i_{SC}) of 17.09 ± 0.20 mA cm⁻², the open-circuit voltage (V_{OC}) was 649 ± 30 mV and a fill factor (ff) of 0.71 ± 0.03 , corresponding to an overall conversion efficiency η , derived from the equation: $\eta = i_{SC} V_{OC} \text{ff}/\text{light intensity}$, 7.88%. Under similar test cell conditions **N719** has shown overall conversion efficiency of 8.03%. In contrast complex **1** and **2** has shown overall conversion efficiency of 1.45 and 4.59%, respectively.

Table 2. Photovoltaic performance of complexes **1-3**.^a

Sensitizer	J_{SC} (mA/cm ²) ^b	V_{OC} (mV) ^b	ff ^b	η (%)
1	5.14	510	55	4.79
2	12.35	585	66	1.45
3	17.09	649	71	7.88
N719	15.91	707	71	8.03

^aPhotoelectrode: TiO₂ (8 + 4 μm and 0.158 cm²). ^bError limits: J_{SC} : ± 20 mA/cm², V_{OC} : ± 30 mV, ff: ± 0.03 .

The high efficiency of complex **3** compared to other two complexes is therefore reasoned to presence of two electron releasing groups substituted at A and B position of PYBI ligand which will tune HOMO-LUMO levels. It seems site A on PYBI ligand to be more influential than site B in terms of exerting enhancement in overall device efficiency. Also in **3**, the planar arrangement at the pyridinyl site would provide extended π -conjugation which in turn leads to red-shifting of absorption spectrum. Moreover the energy gap between singlet and triplet states in complex **3** is lower than **1** & **2** and as a consequence the contribution of triple state for the electron injection is improved. For

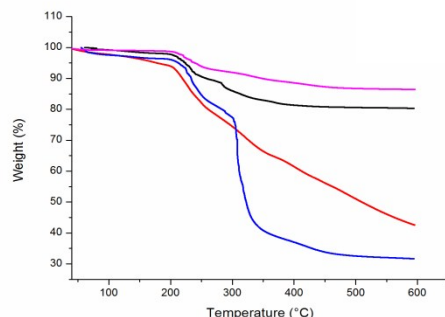


Figure 6. TG/DTG curves of (—)N719, (—) **1**, (—) **2** and (—) **3** with heating rate of 10 °C min⁻¹ under Nitrogen atmosphere.

all above reasons the complex **3** exhibits best efficiency among all three sensitizers.

Finally we have carried out thermal studies in order to understand the thermal properties of these heteroleptic Ru(II) complexes for rooftop applications. For this we have carried out thermo gravimetric analysis of newly synthesized dyes and compared its data to standard N719 sensitizer. Figure 6 shows thermal behaviour of all three Ru(II) sensitizers along with **N719** sensitizer. All these sensitizers are stable up to 200 °C. The weight loss between 200 - 250 °C is attributed to the removal of carboxylic acid group.

In conclusion we have designed and synthesized new heteroleptic Ru(II) polypyridyl complexes based on PYBI ligand. The absorption spectra of complex **3** is red-shifted whereas emission maxima is blue-shifted in comparison with standard **N719** sensitizer. Electrochemical and theoretical properties indicate that LUMO is above TiO₂ conduction band and HOMO is below redox potential of redox couple. When applied to device studies using these newly designed heteroleptic Ru(II) sensitizers, complex **3** has shown an efficiency of 7.88% whereas complex **1** & **2** shown only 1.45 & 4.59%, respectively using I⁻/I₃⁻ redox electrolyte. DFT and TD-DFT calculations have been performed to understand the variations in the device performances of **1**, **2** & **3**. The extended π -conjugation due to planar thiophene moiety at B position, favourable MOs for electron injection and regeneration of dye and better IPCE value for the complex **3** elucidate the high efficiency of **3** than **1** and **2**.

Experimental

Materials and methods

Commercially available reagents and chemicals were procured from sigma-Aldrich. Analytical reagent (AR) grade solvents were used for the reactions while laboratory reagent (LR) grade solvents were used for purifications and column chromatography. ACME silica gel (100-200 mesh) was used for column chromatography. All the reactions were carried out under nitrogen or argon atmosphere using dry and degassed solvents.

Synthesis

The detailed synthetic procedures of ruthenium complexes (**1-3**), their corresponding PYBI precursors (**L1-L3**) and molecular characterizations as follow. Synthesis of 2-(pyridin-2-yl)-1H-benzimidazole was prepared according to literature procedure.³⁴

Synthesis of 5-(2-(pyridin-2-yl)-1H-benzo[d]imidazol-1-yl)thiophene-2-carboxaldehyde (PBI-S-CHO). This important precursor was prepared according to modified literature procedure.³⁴ A Schlenk tube containing N₂ gas was charged with 2-(pyridin-2-yl)-1H-benzimidazole (5.0 mmol), K₂CO₃ (5.5 mmol). Then add liquid reagents 5-bromothiophene-2-carboxaldehyde (6.5 mmol) and solvent DMF (15 mL) purge with N₂ for 10 min and finally the CuI (2.5 mol%) was added. The reaction was kept under an inert atmosphere and placed in preheated oil bath at 160 °C for 16 h. The reaction was quenched by adding saturated sodium chloride and extracted

with DCM. The organic layer was dried over Na_2SO_4 , filtered and evaporated in vacuo to yield the crude product, which was purified by silica gel column chromatography (eluent: Hexane: Ethyl acetate) (78% yield). ^1H NMR (500MHz, CDCl_3) (δ ppm): 9.94(s,1H), 8.43(d,1H), 8.24 (d,1H), 7.90 (d,1H), 7.83 (t,1H), 7.7(d,1H), 7.40 (m, 1H), 7.37 (d,2H), 7.29 (m, 1H), 7.18(d,1H). ESI-MS: calcd m/z ($\text{C}_{17}\text{H}_{11}\text{N}_3\text{OS}$); 305.06; found 306 $[\text{M}+1]^+$.

General procedure for the synthesis of ligands (L1-L2). To the clean and dry two neck RB flask added compound **PBI-S-CHO** (1 mmol), 18-crown-6 (15 mg), and anhydrous K_2CO_3 (2 mmol) in 10 ml of DMF. To this, the solution of corresponding Wittig salt $\text{R-PPh}_3^+\text{Br}^-$ (1.02 mmol)³² in DMF was added slowly with vigorous stirring at room temperature for 2 h. The reaction mixture was poured into ice water to get precipitate then filtered to collect the yellow coloured solid which was dried in high vacuum. The dried solid was dissolved in THF and heated to reflux in the presence of catalytic amount of iodine for overnight. To this added aqueous sodium thiosulphite solution to remove iodine, and extracted with DCM. The distillate organic layer was dried over anhydrous sodium sulphate, filtered and evaporated to dryness. The crude product was purified by column chromatography eluted with hexane: ethyl acetate (yield: 80%).

Ligand 1 (**L1**): Anal. Calcd. for $\text{C}_{36}\text{H}_{26}\text{N}_4\text{S}$ % (546.19): C, 79.09; H, 4.79; N, 10.25. Found C, 79.17; H, 4.80; N, 10.35. ^1H NMR (500MHz, CDCl_3) (δ ppm): 8.59(d,1H), 8.11 (d,1H), 7.91 (d,1H), 7.80(t,1H), 7.28-7.44 (m, 10H), 7.12-7.15 (m, 5H), 7.04-7.09 (m, 4H), 6.97 (d,2H), 6.85 (d,1H). ESI-MS: calcd m/z ($\text{C}_{36}\text{H}_{26}\text{N}_4\text{S}$); 546.19; found 547 $[\text{M}+1]^+$.

Ligand 2 (**L2**): Anal. Calcd. for $\text{C}_{34}\text{H}_{21}\text{N}_3\text{S}$ % (503.15): C, 81.09; H, 4.20; N, 8.34. Found C, 89.10; H, 4.16; N, 8.35. ^1H NMR (500MHz, DMSO-*d*6) (δ ppm): 8.60(d,1H), 8.41 (d,1H), 8.31(d,1H), 8.11-8.15(m,5H), 7.98-8.06 (m, 4H), 7.82-7.94 (m, 3H), 7.45-7.51(m, 2H), 7.33-7.41(m,2H), 7.17(d,1H), 7.02(d, 1H). ESI-MS: calcd m/z ($\text{C}_{34}\text{H}_{21}\text{N}_3\text{S}$); 503.15; found 504 $[\text{M}+1]^+$.

Synthesis of 2-(4-(5-hexylthiophen-2-yl)pyridine-2-yl)-1H-benzimidazole (P-BI-S-NH). *n*-Butyllithium (2.85mmol) was added drop wise to a solution of 2-hexylthiophene (2.38mmol) in dry THF at -78°C under nitrogen atmosphere. The mixture was stirred at this temperature for 1 h, then at RT for 2 h and after cooling to -78°C , tributylstannyl chloride (3.09mmol) was added. After stirring at RT for 5 h, the reaction was quenched by adding saturated ammonium chloride solution. The mixture was extracted with DCM and dried over sodium sulphate. The solvent was evaporated; the crude 2-hexyl-5-tributylstannylthiophene (19.11mmol) was mixed with 2-(4-chloropyridin-2-yl)-1H-benzimidazole²⁶ (14.33mmol) in DMF. The catalyst palladium(II) (0.32mmol) was added to the solution and the mixture was stirred at 85°C under nitrogen for 24 h. After rotary evaporation of DMF, the resulting solid was purified by column chromatography on silica gel using chloroform-hexane as eluent to get the compound (**B**)

(68% yields). ^1H NMR (300MHz, CDCl_3) (δ ppm): 11.23 (bs,1H, -NH), 8.63 (d,1H), 8.57 (d,1H), 7.90 (d,1H), 7.47-7.54 (m,3H), 7.31-7.35 (m,2H), 6.86 (d,1H), 2.88(t,2H), 1.69-1.89 (m,2H), 1.32-1.45 (m,6H), 0.92 (t,3H). ESI-MS: ($\text{C}_{22}\text{H}_{23}\text{N}_3\text{S}$); calcd m/z: [361] found: $[\text{M}+1, 362]$.

Synthesis of ligand L3. To a solution of compound (**P-BI-S-NH**) (0.277mmol) in DMF was added NaH (0.387mmol) portion wise at 0°C . After completion of addition the temperature raised to RT and stirred for 1 h. The reaction mixture was again cooled to 0°C and (2.4mmol) of 3,5-di-*t*-butylbenzyl bromide was added.²⁶ Then the reaction mixture was stirred at 80°C for overnight. After completion of reaction, it was quenched with saturated ammonium chloride at RT, then extracted with ethyl acetate and dried over sodium sulphate. The solvent was removed, the resulting solid was subjected to silica gel column chromatography by eluting with hexane-chloroform to get compound **L3** as white powder (yield 85%). Anal. Calcd. for $\text{C}_{37}\text{H}_{45}\text{N}_3\text{S}$ % (563.33): C, 78.82; H, 8.04; N, 7.45. Found C, 78.85; H, 8.00; N, 7.47. ^1H NMR (300MHz, CDCl_3) (δ ppm): 8.60(d,1H), 8.50(d,1H), 7.83-7.90(m,1H), 7.41-7.47 (m,3H), 7.27-7.33(m,2H), 7.22 (d,1H), 7.05 (d,2H), 6.82(d,1H), 6.11 (d,2H), 2.84 (t,2H), 1.69-1.74 (m,2H), 1.31-1.36 (m,6H), 1.15 (s,18H), 0.89 (t,3H). ESI-MS: calcd m/z ($\text{C}_{37}\text{H}_{45}\text{N}_3\text{S}$); 563.33; found 564 $[\text{M}+1]^+$.

General procedure for the synthesis of ruthenium complexes 1-3. In a typical one-pot synthesis, $[\text{RuCl}_2(\text{p-cymene})_2]$ ⁴² (153 mg, 0.25 mmol) was dissolved in DMF (20 mL), and the corresponding precursor ligand (**L1-L3**) (0.5 mmol) was added. The reaction mixture was heated at 80°C under nitrogen for 4 h; then 4,4'-dicarboxy-2,2'-bipyridine, dcby (0.5 mmol) was added. The reaction mixture was refluxed at 150°C for another 4 h in darkness to avoid photoinduced *cis-trans* isomerization. Excess KNCS was added to the reaction mixture that was heated at 150°C for 5 h. After the reaction, the solvent was removed with a rotary evaporator. Water was added to the resulting mixture to remove excess KNCS. The water-insoluble product was then collected on a sintered-glass crucible with suction filtration, washed with distilled water followed by diethyl ether, and dried in air. The crude complex in basic methanol [with tetrabutyl ammonium hydroxide (TBAOH)] and further purified on a Sephadex LH-20 column with methanol/chloroform mixture as eluent. The main band was collected, concentrated, and precipitated with dilute acidic methanol to obtain pure desired complex.

Complex 1: (yield 48%). ^1H NMR (500MHz, CDCl_3) (δ ppm): 9.49 (d, 1H), 9.01 (s,1H), 8.85 (s, 1H), 8.57 (d, 1H), 8.20 (s, 1H), 7.84 (s, 1H), 7.65 (d, 1H), 7.58 (s, 3H), 7.41 (d, 3H), 7.27-7.32 (m, 6H), 7.03-7.14 (m, 13). ESI-MS: calcd m/z ($\text{C}_{50}\text{H}_{34}\text{N}_8\text{O}_4\text{RuS}_3$); 1008.09; found 1008 $[\text{M}-2(\text{TBA})+\text{H}_2]^+$, 1051 $[\text{M}-2(\text{TBA})+2\text{Na}]^+$.

Complex 2: (yield 52%). ^1H NMR (500MHz, CDCl_3) (δ ppm): 9.68 (d, 1H), 9.43 (d, 1H), 9.00 (d, 2H), 8.80 (s, 1H), 8.47 (m, 1H), 8.40 (d, 1H), 8.28-8.21 (m, 6H), 8.19-8.11 (m, 3H), 7.66-

7.57 (m, 7H), 7.49-7.44 (m, 7H). ESI-MS: calcd m/z ($C_{47}H_{29}N_7O_4RuS_3$); 965.03; found 1003 $[M-2(TBA)+MeOH]^+$.

Complex 3: (yield 55%). 1H NMR (500MHz, $CDCl_3$) (δ ppm): 9.65 (d, 1H), 9.45 (d, 1H), 9.05 (m, 2H), 8.80 (s, 1H), 8.55 (d, 1H), 8.35 (d, 1H), 8.28-8.21 (m, 6H), 7.83-7.90 (m, 1H), 7.41-7.47 (m, 8H), 7.27-7.33 (m, 4H), 7.22 (d, 1H), 7.05 (d, 2H), 6.82 (d, 1H), 6.11 (d, 2H), 3.00-3.55 (m, 9H), 1.69-1.74 (m, 24H), 1.31-1.36 (m, 6H), 1.15 (s, 18H), 0.89 (t, 3H). ESI-MS: calcd m/z ($C_{51}H_{53}N_7O_4RuS_3$); 1025.22; found 1299 $[M+TBA+MeOH]^+$.

Methods

1H -NMR spectra were recorded on a 500MHz INOVA spectrometer. Differential pulse voltammetric measurements were performed on a PC-controlled electrochemical analyser (CH instruments model CHI620C). All these experiments were conducted with 1 mM concentration of compounds in DMF at a scan rate of 10 mV s^{-1} in which tetrabutylammonium hexafluorophosphate (TBAP) is used as a supporting electrolyte. The working electrode was glassy carbon, a standard calomel electrode (SCE) was the reference electrode and Pt wire as an auxiliary electrode. The optical absorption spectra were recorded on a Shimadzu (Model UV-3600) spectrophotometer. Steady-state fluorescence spectra were recorded on a Fluorolog-3 spectrofluorometer (Spex model, JobinYvon) for solutions with optical density at the wavelength of excitation (λ_{ex}) ≈ 0.05 . Thermogravimetric measurements were carried out on a Mettler Toledo TGA/SDTA 851e instrument heating rate at 10 $^\circ C$ min^{-1} with 10 mg of sample under nitrogen atmosphere.

Computational Methodology

Ground state geometries optimized in gas phase with the PBE0⁴³ functional with LanL2DZ⁴⁴⁻⁴⁶ with effective-core potential (ECP) was used for Ru and for rest of the elements 6-311+G(d,p)^{47,48} was used. The conductor-like polarizable continuum model (C-PCM)⁴⁹ was used to optimize the geometries in acetonitrile. TD-DFT (time-dependent density functional theory) calculations were performed on the PBE0 optimized geometries by using CAM-B3LYP⁵⁰ with above mentioned mixed basis set for calculating the vertical excitation energies. All the calculations were done in Gaussian 09.⁵¹ Since, it has been previously reported by many researchers that CAM-B3LYP functional giving reliable results for MLCT.^{52,53} Electronic transitions and molecular orbital compositions were carried out by GaussSum software package.⁵⁴

To study the interaction between the dye and the TiO_2 , a two-dimensional model with 72 TiO_2 units having the dimensions 3x6 in the [101] and [010] directions of cell was applied to simulate anatase TiO_2 (1 0 1) surface. In all calculations the bottom layer of two layer slab was frozen. Atomic positions of the anatase surface with and without sensitizer was optimized by using $1 \times 1 \times 1$ gamma centered k-

point mesh and the optimization of all atomic positions was stopped when the change in the total energy between successive steps was less than 0.04 eV/Å by using Davidson algorithm. A vacuum distance of >15 Å was set in the z-direction to keep negligible interaction between periodic images. Using the plane-wave technique implemented in Vienna ab initio simulation package (VASP).^{55,56} The generalized gradient approximation (GGA) with the PBE⁵⁷ functional has been employed in all calculations. The projector-augmented wave (PAW)^{58,59} method has been applied to describe the electron-ion interaction, and a cut off energy was set to 300 eV.

Device fabrication

The detailed TiO_2 photoelectrode (area: ca. 0.740 cm^2) preparation was described in our earlier studies.^{60,61} Briefly, nanocrystalline TiO_2 films of 8 – 8.5 μm thickness were deposited onto transparent conducting glass (Nippon Sheet Glass, which has been coated with a fluorine-doped stannic oxide layer, sheet resistance of 8-10 Ω/cm^2) over which ~ 4.5 μm thickness of 400 nm anatase TiO_2 particles (CCIC, HPW-400) as scattering layer by screen-printing. These films were gradually sintered at 500 $^\circ C$ for 30 min. The heated electrodes were impregnated with a 0.04 M titanium tetrachloride solution in water saturated desiccator for 30 min at 70 $^\circ C$ and then washed with distilled water and rinsed with ethanol. The electrodes were heated again at 500 $^\circ C$ for 30 min and then allowed to cool to 50 $^\circ C$ before dipping them into the dye solution (3×10^{-4} M in DMF). The electrodes were dipped into the dye solution for 16 h at 25 $^\circ C$. The dye sensitized TiO_2 electrodes were assembled with Pt counter electrodes by heating with a hot-melt surlyn film (Surlyn 1702, 25 μm thickness, Du-Pont) as a spacer in-between the electrodes. A liquid electrolyte was filled through the predrilled hole present on the counter electrode and then the hole was sealed with a Surlyn disk and a thin glass to avoid leakage of the electrolyte. The electrolyte was composed of dimethylpropyl-imidazolium iodide (DMPII), 0.05 M I_2 , TBP 0.5M and 0.1 M LiI in acetonitrile.

The photovoltaic performance of these devices were characterized under irradiation source of 450 W xenon light source (Oriel, Sol 3A, Newport.), which is equivalent to an AM 1.5 solar simulator and was calibrated by using a Tempax 113 solar filter (Schott). In order to reduce scattered light from the edge of the glass electrodes of the dyed TiO_2 layer, a light shading black mask was used onto the DSSCs. For photovoltaic measurements of the DSSCs, the irradiation source was a 450 W xenon light source (Oriel, Sol 3A, Newport) with a filter (Schott 113), whose power was regulated to the AM 1.5G solar standard by using a reference Si photodiode equipped with a colour matched filter in order to reduce the mismatch in the region of 350-750 nm between the simulated light and AM 1.5G to less than 4%. The measurement of incident photon-to-current conversion efficiency (IPCE) was plotted as a function of excitation wavelength by using the incident light from a 300 W xenon lamp (ILC Technology, USA), which was focused through a Gemini-180 double monochromator (Jobin Yvon

Ltd.). The measurement settling time between applying a voltage and measuring a current for the I-V characterization of DSSCs was fixed to 40 ms.

Acknowledgements

The authors are thanks to CSIR-NISE for financial support to carry out this work. YS thanks to BRNS (DAE) for financial support.

References

1. B. O'Regan, M. Grätzel, *Nature*, 1991, **353**, 737-740.
2. M. Grätzel, *Acc. Chem. Res.* 2009, **42**, 1788-1798.
3. S. Zhang, X. Yang, Y. Numata, L. Han, *Energy Environ. Sci.*, 2013, **6**, 1443-1464.
4. G. D. Barber, P. G. Hoertz, S.-H. A. Lee, N. M. Abrams, J. Mikulca, T. E. Mallouk, P. Liska, S. M. Zakeeruddin, M. Grätzel, A. Ho-Baillie, M. A. Green, *J. Phys. Chem. Lett.* 2011, **2**, 581-585.
5. Y. Chi, K.-L. Wu, T.-C. Wei, *Chem. Asian J.* 2015, **10**, 1098-1115.
6. T. Kinoshita, J. T. Dy, S. Uchida, T. Kubo H. Segawa, *Nat. Photonics*, 2013, **7**, 535-539.
7. Q. Wang, S. Ito, M. Grätzel, F. Fabregat-Santiago, I. Mora-Seró, J. Bisquert, T. Bessho, H. Imai, *J. Phys. Chem. B* 2006, **110**, 25210-25221.
8. A. Yella, H.-W. Lee, H. N. Tsao, C. Yi, A. K. Chaniran, M. K. Nazeeruddin, E. W.-G. Diau, C.-Y. Yeh, S. M. Zakeeruddin, M. Grätzel, *Science*, 2011, **334**, 629-634.
9. S. Mathew, A. Yella, P. Gao, R. Humphry-Baker, B. F. E. Curchod, N. Ashari-Astani, I. Tavernelli, U. Rothlisberger, M. K. Nazeeruddin and M. Grätzel, *Nature*, 2014, **6**, 242-247.
10. L.-L. Lia, E. W.-G. Diau, *Chem. Soc. Rev.*, 2013, **42**, 291-304.
11. P. Y. Reddy, L. Giribabu, C. Lyness, H. J. Snaith, C. Vijaykumar, M. Chandrasekharam, M. Lakshmikantam, J.-H. Yum, K. Kalyanasundaram, M. Grätzel, M. K. Nazeeruddin, *Angew. Chem. Int. Ed.*, 2007, **46**, 373-376.
12. J.-J. Cid, J.-H. Yum, S.-R. Jang, M. K. Nazeeruddin, E. Martínez-Ferrero, E. Palomares, J. Ko, M. Grätzel, and T. Torres, *Angew. Chem. Int. Ed.*, 2007, **46**, 8358-8362.
13. Z. Ning, Y. Fu, H. Tian, *Energy Environ. Sci.* 2010, **3**, 1170-1181.
14. M. Zhang, Y. Wang, M. Xu, W. Ma, R. Li, P. Wang, *Energy Environ. Sci.* 2013, **6**, 2944-2949.
15. A. Hagfeldt, G. Boschloo, L. Sun, L. Kloo, H. Pettersson, *Chem. Rev.* 2010, **110**, 6595-6663.
16. N. J. Jeon, J. H. Noh, W. S. Yang, Y. C. Kim, S. Ryu, J. Seo, S. Seok, *Nature*, 2015, **517**, 476-480.
17. O. Kohle, M. Grätzel, A. F. Meyer, T. B. Meyer, *Adv Mater.* 1997, **9**, 904-906.
18. H. Ozawa, R. Shimizu, H. Arakawa, *RSC Adv.*, 2012, **2**, 3198-3200.
19. P. Wang, S. M. Zakeeruddin, J. E. Moser, M. K. Nazeeruddin, T. Sekiguchi, M. Grätzel, *Nat. Mater.*, 2003, **2**, 402-407.
20. P. Wang, S. M. Zakeeruddin, P. Comte, R. Charvet, R. Humphry-Baker, M. Grätzel, *J. Phys. Chem. B*, 2003, **107**, 14336-14341.
21. C.-Y. Chen, J.-G. Chen, S.-J. Wu, J.-Y. Li, C.-G. Wu, K.-C. Ho, *Angew. Chem. Int. Ed.*, 2008, **47**, 7342-7345.
22. F. Gao, Y. Wang, D. Shi, J. Zhang, M. Wang, X. Jing, R. Humphry-Baker, P. Wang, S. M. Zakeeruddin, M. Grätzel, *J. Am. Chem. Soc.*, 2008, **130**, 10720-10728.
23. Y. Cao, Y. Bai, Q. Yu, Y. Cheng, S. Liu, D. Shi, F. Gao, P. Wang, *J. Phys. Chem. C*, 2009, **113**, 6290-6297.
24. Q. Yu, S. Liu, M. Zhang, N. Cai, Y. Wang, P. Wang, *J. Phys. Chem. C*, 2009, **113**, 14559-14566.
25. Q. Yu, Y. Wang, Z. Yi, N. Zu, J. Zhang, M. Zhang, P. Wang, *ACS Nano*, 2010, **4**, 6032-6038.
26. W.-K. Huang, H.-P. Wu, P.-L. Lin, E. W.-G. Diau, *J. Phys. Chem. C* 2013, **117**, 2059-2065.
27. Y. Q. Li, M. K. Fung, Z. Xie, S.-T. Lee, L.-S. Hung, J. Shi, *Adv. Mater.* 2002, **14**, 1317-1321.
28. Q. Wang, Z. Zhang, S. M. Zakeeruddin, M. Grätzel, *J. Phys. Chem. C*, 2008, **112**, 7084-7092.
29. L. Giribabu, C. V. Kumar, C. S. Rao, V. G. Reddy, P. Y. Reddy, M. Chandrasekharam, Y. Soujanya, *Energy Environ. Sci.*, 2009, **2**, 770-773.
30. L. Giribabu, T. Bessho, M. Srinivasu, C. V. Kumar, Y. Soujanya, V. G. Reddy, P. Y. Reddy, J.-H. Yum, M. Grätzel, M. K. Nazeeruddin, *Dalton Trans.*, 2011, **40**, 4497-4504.
31. L. Giribabu, V. K. Singh, M. Srinivasu, Ch. V. Kumar, V. G. Reddy, Y. Soujanya, P. Y. Reddy, *J. Chem. Sci.*, 2011, **123**, 371-378.
32. W. W. Wadsworth, W. D. Emmons, *J. Am. Chem. Soc.*, 1961, **83**, 1733-1738.
33. J. K. Stille, *Angew. Chem. Int. Ed. Eng.* 1986, **25**, 508-524.
34. W.-K. Huang, H.-P. Wu, P.-L. Lin, Y.-P. Lee, E. W.-G. Diau, *J. Phys. Chem. Lett.*, 2012, **3**, 1830-1835.
35. K.-L. Wu, Y. Hu, C.-T. Chao, Y.-W. Yang, T.-Y. Hsiao, N. Robertson, Y. Chi, *J. Mater. Chem. A* 2014, **2**, 19556-19565.
36. F.-C. Hu, S.-W. Wang, Y. Chi, N. Robertson, T. Hewat, Y. Hu, S.-H. Liu, P.-T. Chou, P.-F. Yang, H.-W. Lin, *ChemPhysChem*. 2012, **15**, 1207-1215.
37. H.-Y. Hsu, C.-W. Chen, W.-K. Huang, Y.-P. Lee, E. W.-G. Diau, *J. Phys. Chem. C*, 2014, **118**, 16904-16911.
38. S. P. McGlynn, T. Azumi and M. Kinoshita, *Molecular Spectroscopy of the Triplet State*, Prentice Hall, NJ, 1969.
39. R. Lincoln, L. Kohler, S. Monro, H. Yin, M. Stephenson, R. Zong, A. Chouai, Ch. Dorsey, R. Hennigar, R. P. Thummel, S. A. McFarland, *J. Am. Chem. Soc.* 2013, **135**, 17161-17175.
40. K. L. McCall, A. Morandeira, J. Durrant, L. J. Yellowless, N. Robertson, *Dalton Trans.* 2010, **39**, 4138-4145.
41. K. Momma and F. Izumi, "VESTA: a three-dimensional visualization system for electronic and structural analysis," *J. Appl. Crystallogr.*, 2008, **41**, 653-658.
42. D. Kaung, C. Klein, Z. Zhang, S. Ito, J.-E. Moser, S. M. Zakeeruddin, M. Grätzel, *Small*, 2007, **3**, 2094-2102 (and references therein).
43. C. Adamo and V. Barone, *J. Chem. Phys.*, 1999, **110**, 6158-6169.
44. P. J. Hay, W. R. Wadt, *J. Chem. Phys.*, 1985, **82**, 270-283.
45. W. R. Wadt, P. J. Hay, *J. Chem. Phys.*, 1985, **82**, 284-298.

46. P. J. Hay, W. R. Wadt, *J. Chem. Phys.*, 1985, **82**, 299-310.
47. R. Krishnan, J. S. Binkley, R. Seeger, J. A. Pople, *J. Chem. Phys.*, 1980, **72**, 650-654.
48. T. Clark, J. Chandrasekhar, P. V. R. Schleyer, *J. Comp. Chem.*, 1983, **4**, 294-301.
49. M. Cossi, N. Rega, G. Scalmani, V. Barone, *J. Comput. Chem.*, 2003, **24**, 669-681.
50. T. Yanai, D. P. Tew, N. C. Handy, *Chem. Phys. Lett.*, 2004, **393**, 51-57.
51. M. J. Frisch *et al.*, *Gaussian09 Revision C.01*, Gaussian, Inc., Wallingford CT, 2010.
52. T. Yanai, D. P. Tew and N. C. Handy, *Chem. Phys. Lett.*, 2004, **393**, 51-57.
53. M. J. G. Peach, P. Benfield, T. Helgaker, D. J. Tozer, *J. Chem. Phys.*, 2008, **128**, 044118.
54. N. M. O'Boyle, A. L. Tenderholt, K. M. Langner, *J. Comput. Chem.*, 2008, **29**, 839-845.
55. G. Kresse, J. Hafner, *Phys. Rev. B: Condens. Matter Mater. Phys.*, 1993, **47**, 558-561.
56. G. Kresse, J. Furthmüller, *Comput. Mater. Sci.*, 1996, **6**, 15-50.
57. J. P. Perdew, K. Burke, M. Ernzerhof, *Phys. Rev. Lett.*, 1996, **77**, 3865-3868.
58. P. E. Blöchl, *Phys. Rev. B: Condens. Matter Mater. Phys.*, 1994, **50**, 17953-17979.
59. G. Kresse, J. Furthmüller, *Phys. Rev. B: Condens. Matter Mater. Phys.*, 1999, **54**, 1758-1775.
60. L. Giribabu, Ch. V. Kumar, V. G. Reddy, P. Y. Reddy, Ch. S. Rao, S. -R. Jang, J. -H. Yum, M. K. Nazeeruddin, M. Grätzel, *Sol. Energy Mater. Sol. Cells*, 2007, **91**, 1611-1617.
61. L. Giribabu, V. K. Singh, Ch. V. Kumar, Y. Soujanya, P. Y. Reddy, M. L. Kantam, *Solar Energy* 2011, **85**, 1204-1212.